Numerical Simulation of Vortex Shedding Past a Circular Cylinder in a Cross-Flow at Low Reynolds Number With Finite Volume-Technique: Part 1 - Forced Oscillations

Antoine Placzek, Jean-François Sigrist, Aziz Hamdouni

NUMERICAL SIMULATION OF VORTEX SHEDDING PAST A CIRCULAR CYLINDER IN A CROSS-FLOW AT LOW REYNOLDS NUMBER WITH FINITE VOLUME-TECHNIQUE. PART 1: FORCED OSCILLATIONS

Antoine PLACZEK

DCN Propulsion
Service Technique et Scientifique
DCN Propulsion
44620 LA MONTAGNE, France

Laboratoire d'Etude des Phénomènes de Transfert
Appliqués au Bâtiment - Université de La Rochelle
Avenue Michel CREPEAU
17042 LA ROCHELLE Cedex 1, France

Jean-François SIGRIST

Service Technique et Scientifique
DCN Propulsion
44620 LA MONTAGNE, France
jean-francois.sigrist@dcn.fr

Aziz HAMDOUNI

Laboratoire d'Etude des Phénomènes de Transfert
Appliqués au Bâtiment - Université de La Rochelle
Avenue Michel CREPEAU
17042 LA ROCHELLE Cedex 1, France

ABSTRACT

The numerical simulation of the flow past a circular cylinder forced to oscillate transversely to the incident stream is presented here for a fixed Reynolds number equal to 100. The 2D Navier-Stokes equations are solved with a classical Finite Volume Method with an industrial CFD code which has been coupled with a user subroutine to obtain an explicit staggered procedure providing the cylinder displacement. A preliminary work is conducted in order to check the computation of the wake characteristics for Reynolds numbers smaller than 150. The Strouhal frequency f_S, the lift and drag coefficients C_L and C_D are thus controlled among other parameters. The simulations are then performed with forced oscillations f_0 for different frequency ratios $F=f_0/f_S$ in [0.50-1.50] and an amplitude A varying between 0.25 and 1.25. The wake characteristics are analysed using the time series of the fluctuating aerodynamic coefficients and their FFT. The frequency content is then linked to the shape of the phase portrait and to the vortex shedding mode. By choosing interesting couples (A,F), different vortex shedding modes have been observed, which are similar to those of the Williamson-Roshko map.

1. INTRODUCTION

Flow around a fixed or oscillating cylinder has received continued attention in the past few decades. In addition to being a building block in the understanding of bluff body dynamics, it has a large number of applications in many engineering situations. This study is a prelude to investigate the feasibility of coupled fluid-structure computations with an industrial CFD code that could be used later on a tube bundle configuration, like those existing in nuclear steam generators.

The wake of a circular cylinder exhibits a large variety of phenomena very rich and complex which come from the diverse instabilities growing in the near wake. It is well-known that for Reynolds numbers smaller than 50, two recirculation zones attached to the cylinder wall can be observed. As the Reynolds number is increased the wake consists of two staggered rows of vortices forming the classical Von-Karman streets, the vortices of each row being shed alternately from either side of the cylinder. For larger Reynolds numbers, three dimensional structures appear in the wake which becomes progressively turbulent. The classification of the different regimes is not simple and changes according to the authors. The main reason is due to the fact that the wake is very sensitive to the experimental system or the numerical model. A rather clear classification can be found in [23].

The flow around an oscillating cylinder is even more complex, because of the interaction between the vortex shedding phenomenon and the cylinder displacement. Indeed, as the vortices are shed, a periodic force is exerted on the cylinder, whose component in the transverse direction (lift force) has the same frequency as the vortex-shedding cycle, while the frequency of its streamwise direction (drag force) is equal to twice the shedding frequency. In certain ranges of amplitude and frequency of oscillation, the body motion can control the instability mechanism which leads to vortex shedding. One of the most interesting characteristics of this fluid-structure interaction is the synchronization, or "lock-in",

between the vortex shedding and vibration frequencies. The vortex shedding frequency diverges from that corresponding to a fixed cylinder and becomes equal to the natural frequency of the cylinder, when the oscillation amplitude exceeds a critical threshold.

This complicated fluid-structure interaction phenomenon still draws the attention of researchers and has become the typical test case for new numerical methods. A lot a study involving RANS, LES or DNS simulations using Finite Element or Finite Volume methods to solve the Navier-Stokes equations can be found in the literature [1], [5], [14], [21] and many others, for a large interval of Reynolds numbers. It is also crucial to check that the numerical computation lead to the same phenomena than those observed in experimental works like [3], [11].

The numerical model used for the computations is first presented; results obtained for the fixed cylinder are then briefly exposed; cylinder response to forced oscillations is then investigated.

2. NUMERICAL MODEL

2.1. Computation of the Navier-Stokes equations

The flow is assumed to be Newtonian, incompressible, and laminar as the Reynolds number is small ($\mathrm{Re} < 150$). The integral form of a conservation equation for any fluid variable ϕ (pressure, velocity) written on a moving domain $\Omega(t)$ is the following:

$$\frac{d}{dt}\int_{\Omega(t)} \rho\phi d\Omega + \int_{\partial\Omega(t)} \rho(u_j - w_j^*)\phi d\mathbf{n}_j = \int_{\Omega(t)} S_\phi d\Omega + \int_{\partial\Omega(t)} \Gamma \frac{\partial\phi}{\partial x_j} d\mathbf{n}_j \quad (\mathbf{1})$$

Equation (1) is discretised using a Finite Volume method on a 2D mesh, i.e. the conservation equation (1) is written for each cell of the fluid domain. The grid velocity w_i^* appearing in the left side of (1) is deduced from the known node displacement imposed by the cylinder displacement and becomes then a source term on the right-hand side. The time dependent term in (1) is approximated by an Euler scheme. Diffusive and convective fluxes are calculated using finite difference approximations. The pressure corrections are taken into account thanks to the SIMPLE algorithm for steady computations and the PISO pocedure in unsteady cases. Finally, an algebraic system is obtained and solved iteratively until the convergence is reached. More details on the discretisation scheme and the resolution of the algebraic system can be found in [7] and [20].

2.2. Cylinder displacement and moving mesh

A sinusoidal motion is explicitly imposed to the cylinder in a user subroutine handled by the CFD code at each time step before solving the flow field. The displacement parameters are the frequency f_o and the amplitude of oscillation $A = y_{\max}/d$. The vertical motion is thus governed by the following equation:

$$y(t) = A\sin(2\pi f_o t) \quad (\mathbf{2})$$

The cylinder oscillates independently from the flow but the wake can be strongly affected by the cylinder motion. The different wake regimes are classified thanks to the frequency ratio *F* defined below:

$$F = \frac{f_0}{f_S} \quad (\mathbf{3})$$

where f_S refers to the Strouhal frequency for the fixed cylinder, i.e. the vortex shedding frequency.

The movement of the cylinder is taken into account in the fluid model which has been formulated in an Arbitrary Lagrangian Eulerian (ALE) formulation. In this way, the mesh can be updated from the knowledge of the wall cylinder motion. The moving mesh algorithm used has been adapted from the one developed in [19]. The displacements and velocities of each cell of the interior moving mesh are then computed to respect the mesh quality to the maximum. This algorithm has been used successfully in [19] and [20] and as the amplitude of oscillation remains here small, there is no important mesh distortion.

Finally, the no-slip condition on the cylinder wall Γ has to be adapted. For each node in contact with the cylinder wall, the fluid velocity $\mathbf{u} = (u, v)$ is explicitly set equal to the cylinder velocity $\mathbf{y}(t)$ so that the cinematic coupling condition is respected:

$$v(t) = \dot{y}(t) \qquad \forall M \in \Gamma \quad (\mathbf{4})$$

2.3. Geometry and boundary conditions

The computational domain is represented on the Fig. 1. The cylinder position has been chosen so that the downstream length is long enough to observe the vortex shedding which should not be influenced by the outlet boundary condition. The mesh is block-structured and a ring has been introduced around the cylinder. In order to reduce the computation time, the mesh only moves in the interior of this ring (represented with a dash line on Fig. 1). As the mesh has been refined near the cylinder wall with a ratio in the ring, the total number of cells stands at 28800.

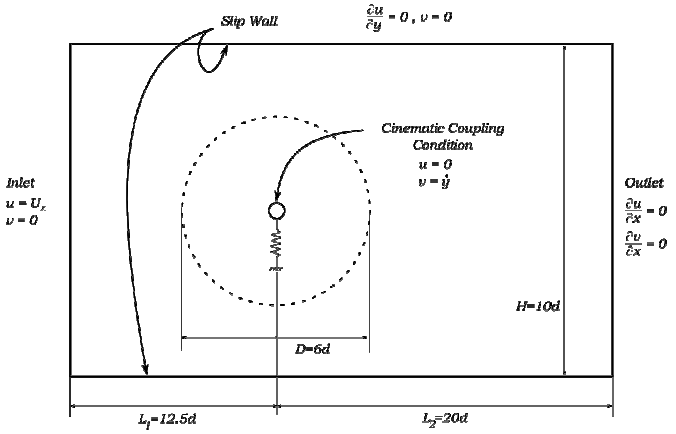

Figure 1. Geometry and boundary conditions of the computational domain

3. FIXED CYLINDER WAKE

The wake of a fixed cylinder is investigated here for four Reynolds numbers in the permanent regime ($5 < \mathrm{Re} < 50$) and four others in the 2D periodic regime ($50 < \mathrm{Re} < 150$). The mesh remains fixed and several characteristic parameters of the wake are checked to control the validity of the numerical model.

3.1. Results in permanent regime

The simulations are carried out in permanent regime until the convergence residual becomes smaller than 10^{-7}. The Reynolds numbers investigated are 10, 20, 30 and 40, all below the bifurcation between the permanent and the periodic regime. In this regime, the wake is characterized by two recirculation zones *attached* to the cylinder wall. These zones are recognizable by the strong vorticity, which is due to the fact that the flow is rotational, and by low pressure levels, as it can be seen on Fig. 2.

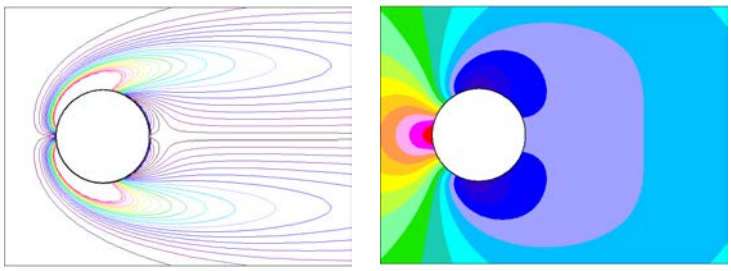

Figure 2. Vorticity and pressure contours at Re=40

The first parameter controlled is the length L_r of the recirculation zone which is defined by the downstream distance where the velocity is null. Then the values of the separation angle θ_S are checked. θ_S is defined by the angular position on the cylinder wall where the vorticity is null. The evolution of these two parameters is deduced from the graphs plotted on Fig. 3. The values obtained for L_r are compared to those found in [2], [9]; the separation angle is compared to the results of [4] and [9], see Tab. 1. The errors remain inferior to 5% for all Reynolds numbers.

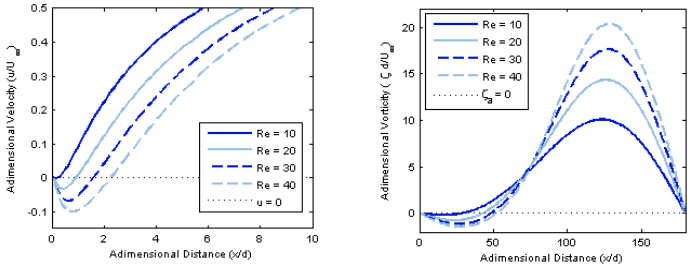

Figure 3. Plots used for the determination of the recirculation length and angle of separation

The values of the drag C_D and suction coefficients C_A are also controlled. As expected, the lift coefficient C_L remains null because of the perfect symmetry of the flow field. The expressions of the aerodynamic coefficients are given below:

$$C_D = \frac{F_D}{1/2\rho U_\infty^2 dl} \quad C_L = \frac{F_L}{1/2\rho U_\infty^2 dl} \quad C_a = \frac{p_\infty - p_0}{1/2\rho U_\infty^2} \qquad (5)$$

F_D (resp. F_L) is the drag force (resp. the lift force), p_∞ is the reference pressure and p_o is the pressure at the rear stagnation point. The values found for the aerodynamic coefficients are also in good agreement (comparison with [2], [9] and [10]) although the error on C_A is slightly higher but remains under 10%. This can be explained by the fact that C_A is a local variable which is from the computational point of view very sensitive to numerical errors.

Table 1. Values of the geometric characteristics and force for the permanent regime

Reynolds number	10	20	30	40
Recirculation length L_r/d	0.250	0.934	1.603	2.265
Separation angle θ_s	28.4	47.2	48.6	52.5
Drag coefficient C_D	3.02	2.16	1.81	1.60
Suction coefficient C_A	0.67	0.54	0.50	0.48

3.2. Results in periodic vortex shedding regime

Transient simulations are now investigated. The simulation time is chosen long enough to observe about fifteen vortices shedding once the periodic regime is established. The time step is set to about 1/150 of the Strouhal period during the transient phase at the beginning of the computation. To obtain the Von Karman streets, the symmetry of the wake has to be

numerically broken. This is done by introducing a 1% amplitude arbitrary noise on the incident velocity. This perturbation is only maintained during a small time interval. Once the periodic regime is reached, the time step is divided by 4 to increase the accuracy of the results. The CPU time stand at about 26h. The Reynolds numbers tested now are 60, 80, 100 and 120. In this case, the wake consists of two staggered rows of vortices being shed alternately from either side of the cylinder. Figure 4 shows the vorticity contours in the wake of the cylinder over a Strouhal period. At $t = t_0$, a vortex is forming in the lower side of the wake and is then completely detached from the cylinder wall at $t = t_0 + 1/3T_S$. At $t = t_0 + 2/3T_S$, the vortex of the upper side is about to be inserted between the lower vortex formed previously and a new vortex which is forming. At $t = t_0 + T_S$, the vortex in the upper side is completely detached and the wake topology is exactly the same as the one observed at $t = t_0$.

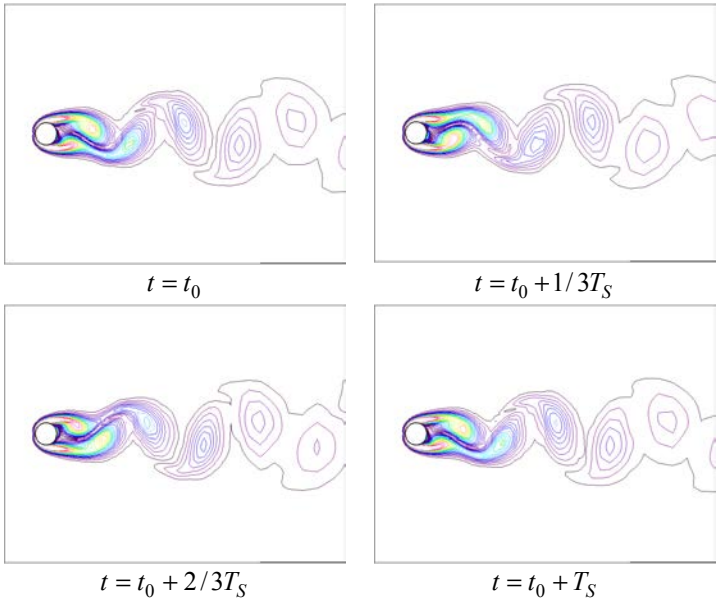

Figure 4. Vorticity contours in the wake over one Strouhal period

The periodicity of the shedding leads naturally to the fluctuation of the aerodynamic coefficients. The convergence of the coefficients is show on Fig. 5 for $\mathrm{Re} = 100$. The first part of the computation ($t^* < 10$) corresponds to the transient phase during which the perturbation arrives on the cylinder. The periodic state is then reached and it can be seen that the drag coefficient oscillates at twice the lift or suction coefficient frequency.

The Strouhal frequency f_S can be defined as the lift coefficient frequency or the fluctuation frequency of velocity for any point in the near wake. The two frequencies are the same and the Strouhal number is obtained by the following relation:

$$S_t = f_S \frac{d}{U_\infty} \qquad (6)$$

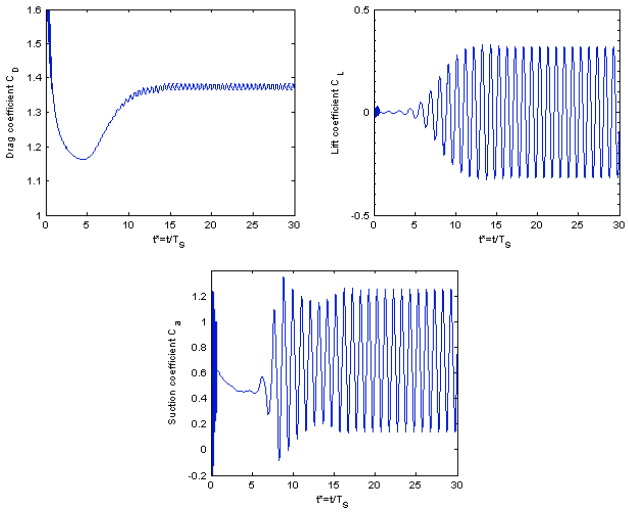

Figure 5. Convergence of the aerodynamic coefficients at Re=100

Many empirical expressions have been proposed for the evaluation of the Strouhal number [8], [15], [18], [22]. The value obtained here is slightly greater than in other studies and this could be explained by the small aspect ratio H/d used in the simulations. The mean values of the drag and suction coefficients are computed over several periods in the periodic regime (without the transient phase). The mean value of the lift is null and we therefore use the maximal value reached or the root mean square value. The values of the parameters controlled are listed in Tab. 2 with the Strouhal number. The aerodynamic coefficients are compared to the results of [9] and with [15], who gives an empirical relation for the rms lift coefficient. Our results are still in very good agreement with other studies, even if the Strouhal number is slightly greater.

Table 2. Values of the Strouhal number and force coefficients for the periodic regime

Reynolds number	60	80	100	120
Strouhal number St	0.141	0.158	0.169	0.177
Mean drag Coefficient C_D	1.44	1.40	1.37	1.35
Max. lift coefficient $C_{L,max}$	0.12	0.25	0.33	0.39
RMS lift coefficient $C_{L,rms}$	0.08	0.18	0.23	0.28
Mean suction coefficient. C_a	0.54	0.62	0.70	0.75

This first series of simulations has shown that the CFD code is able to give an accurate description of the flow field around a fixed cylinder. The geometric vortex shedding

characteristics and the intensity of the pressure and aerodynamic forces are very well evaluated.

4. FORCED OSCILLATIONS

Simulations are then performed for a cylinder forced to oscillate at the frequency f_o which is better described with the frequency ratio $F = f_o / f_S$. Computations are run from the solution for the fixed cylinder, i.e. when the Von Karman streets are already present. The Reynolds number is kept constant and equal to 100 and only the natural frequency f_o and possibly the amplitude A are changed.

The lock-in zone is defined by the domain where the vortex shedding frequency diverges from the value expected at the Reynolds number considered and locks on the frequency of the forced oscillations: this zone is represented Fig. 6.

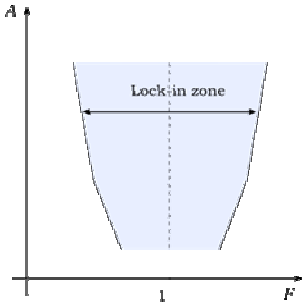

Figure 6. Lock-in zone for forced transverse oscillations

If the amplitude is kept constant and F varies over a wide enough interval, the lock-in zone should be crossed and the different regimes should be observed.

4.1. Cylinder response and lock-in zone

The cylinder response is studied for several frequency ratios F between 0.50 and 1.50 while the amplitude A is kept constant and equal to 0.25. We present in the following two types of responses, the first in the lock-in zone and the second out of the lock-in zone. For $A = 0.25$, the upper and lower limits are approximately located at $F = 0.75$ and $F = 1.25$ [13].

- **Locked configurations**

Two cases are presented here: $F = 0.90$ and $F = 1.10$. The time evolutions of the aerodynamic coefficients show a strong increase of the amplitude for each coefficient and a pure sinusoidal response which is clearly highlighted with a FFT. The spectra of the lift coefficient presented on Fig. 7 show that the main frequency is found at $f^* = 1.0$, where $f^* = f / f_o$. This indicates that the aerodynamic forces are governed by the forced frequency (FFTs of the drag coefficient not represented here would show a main peak at $f^* = 2.0$). This periodicity can also be observed in the wake: visualisations of the vorticity contours in the wake are exactly the same at two moments separated by one natural period $T_o = 1/f_o$.

The phase portraits of the system are a very practical tool to analyse the response. Phase portraits for the two cases under study are thus given on Fig. 7. The existence of a limit cycle is the result of the perfect sinusoidal response and the inclination of the cycle gives an estimation of the phase angle between the imposed displacement and the lift. Finally, the sense of the cycle is clockwise, which means that the energy transfer takes place from the fluid to the cylinder.

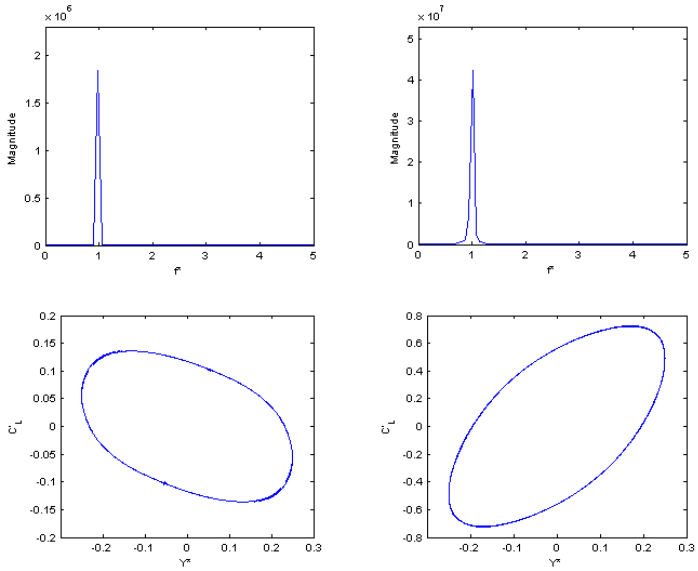

Figure 7. FFT of the lift coefficient (top) and phase portraits (bottom) for F=0.90 (left) and F=1.10 (right)

- **Unlocked configurations**

The frequency ratios $F = 0.50$ and $F = 1.50$ lead to an unlocked wake. The pure sinusoidal response in the time evolution of the aerodynamic coefficients is lost and a beating behaviour is observed. The FFTs of the lift coefficient are now composed of two main peaks even if it is not very clear at $F = 1.50$ (see Fig. 8, top). The peak at $f^* = 1$, which corresponds to the forced oscillation frequency f_o, is still here and is still the main peak at $F = 1.50$. The second peak comes from the Strouhal frequency f_S evaluated for the fixed cylinder. The two frequencies are now present but the main peak is alternately that corresponding to f_o or f_S.

The phase portraits (Fig. 8, bottom) are dramatically different from those obtained earlier. There is still a limit

cycle but the path is different between two cycles and as a result, there are many ways in the interior of the cycle. This should be related to the beating behaviour which causes a fluctuation of the C_L value between two successive cycles.

Like in [14], we choose to define the lock-in region as the domain where the evolution of C_L is purely sinusoidal and governed by the forced oscillation frequency. This means that there is only one peak at $f^* = 1$ in the FFT. The presence of only one peak is immediately visible according to the shape of the phase portrait and, combined with the FFT, it is a practical tool to define when lock-in is observed or not.

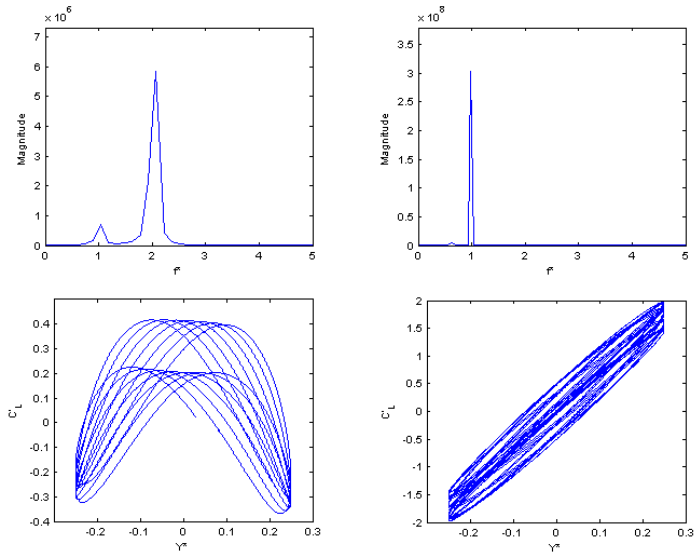

Figure 8. FFTs of the lift coefficient (top) and phase portraits (bottom) for F=0.50 (left) and F=1.50 (right)

If we define T_B as the beating period, the following relations between the different periods can be written:

$$\begin{aligned} F = 0.50 \qquad & T_B = T_0 = \frac{1}{F} T_S \\ F = 1.50 \qquad & T_B = 8T_0 = \frac{8}{F} T_S \end{aligned} \tag{7}$$

The beating period is absent from the spectra but it plays an important role for the vortex shedding process. The visualizations of the contours of vorticity at different time steps show that the wake is similar at two instants separated by a beating period. Figure 9 represents the vorticity contours at $t = t_o$, $t = t_o + T_o$, $t = t_o + T_S$, and $t = t_o + T_B$. It is clear that the periodicity of the wake is governed by the beating period (the first and last pictures are exactly the same) instead of the Strouhal period T_S or the forced oscillation period T_o as it could be expected by seeing the FFT. Inside the lock-in zone, the wake was governed by the period T_o of the forced oscillation. This period was also the period of the lift coefficient fluctuations. Outside the lock-in zone, the behaviour is more complex: the lift coefficient is characterized by the Strouhal frequency below the lower limit of the lock-in zone (resp. the forced oscillation frequency upon the upper limit) but the wake is governed by the beating period which is a multiple of the forced oscillation period.

In addition to a shift of the shedding frequency, the lock-in region is also characterized by an increase of the aerodynamic coefficients, when compared to the fixed cylinder case. The mean drag is practically always greater than the fixed cylinder value whereas the rms lift coefficient is smaller at the beginning of the lock-in zone and increases gradually through as F increases. At the end of the lock-in zone, the lift amplification seems to become less pronounced. The evolution of these parameters is presented on Fig. 10 where the dash line represents the fixed cylinder value. The evolution of the mean suction coefficient is not given as it is quite similar to the mean drag coefficient with a maximal value at $F = 1.10$.

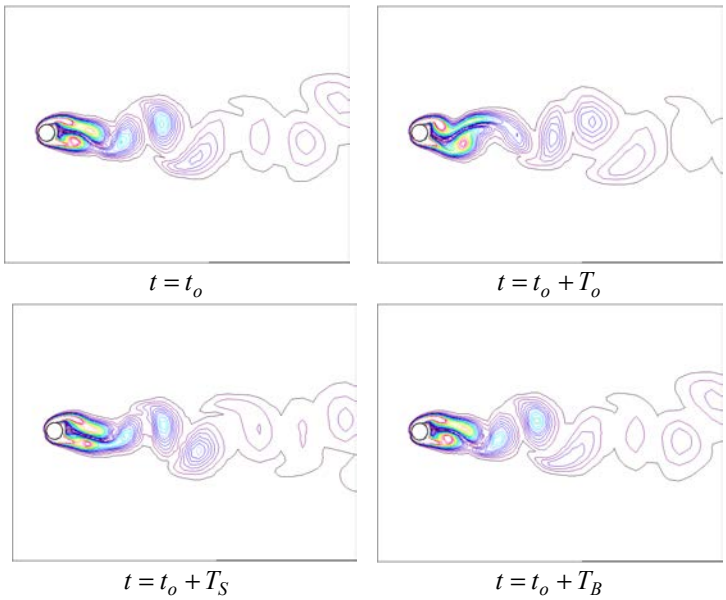

Figure 9. Vorticity contours at different strategic moments for F=1.50

To conclude this first paragraph, it is worth mentioning that a jump in the phase angle should be observed at the beginning of the lock-in zone. In [3], the authors find experimentally a jump in the phase angle ϕ and the lift coefficient at about $F = 0.80$. Below this value, ϕ is approximately equal to 180° and sinks to 0° at the critical value of F. The authors attribute this jump to a modification of vortex shedding mode which appears in the wake. In the present study, it is also observed that the lift coefficient increases when F increases but [3] found out that the steepest slope is at $F = 0.80$, whereas in the present case this happens later, between $F = 1.00$ and 1.25. The phase angle has only

been evaluated in the lock-in zone where the fluctuations are purely sinusoidal. The present simulations show a smooth decrease of ϕ with F and no real jump has been observed. The first reason is that only three cases where treated in the lock-in zone which lead to the values $\phi = 113.8$, $\phi = 80.5$ and $\phi = 47.7$ for $F = 0.90$, $F = 1.00$ and $F = 1.10$. A second and probably more subtle reason is the difference in the Reynolds number between our study ($\mathrm{Re} = 100$) and [3] ($\mathrm{Re} = 2300$). Although it is not yet clear, it has been noticed [12] that the change of vortex shedding mode is most of the time not observed [1], [14] at low Reynolds numbers, whereas it can be seen at higher Reynolds numbers [23].

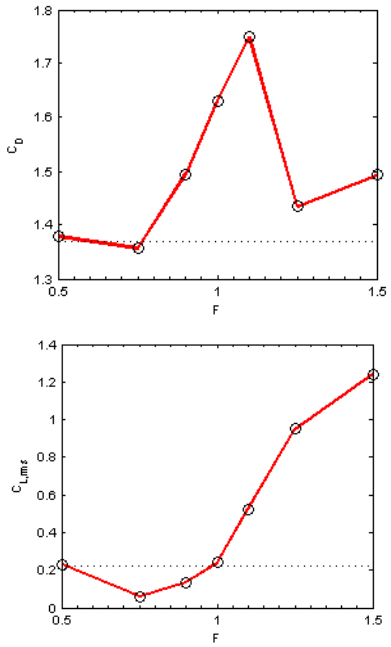

Figure 10. Evolution of the mean drag and rms lift coefficients with F

4.2. Vortex shedding modes

Attention is now paid to the topology of the wake: first the beating phenomenon is analysed and associated to a vortex merging mechanism at $F = 1.25$; then greater values for the amplitude A are used to observe different shedding modes, which are commonly called the 2P and P+S modes.

- **Vortex merging**

At $F = 1.25$ and $A = 0.25$, a beating phenomenon similar to those observed earlier appear. The beating period T_B spread over seven forced oscillation periods T_o. This beating behaviour could be explained by a vortex merging mechanism which causes the break of periodicity in the time histories of the aerodynamic coefficients. To understand it, we focus on the time interval $[t_o + 2T_o, t_o + 4T_o]$ comprised in a beating period.

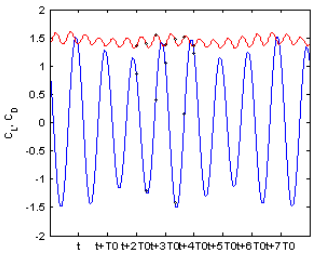

C_L and C_D fluctuations over the beating period

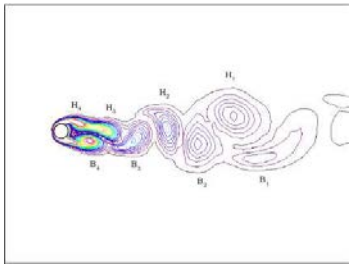

$t_o + 2T_o$

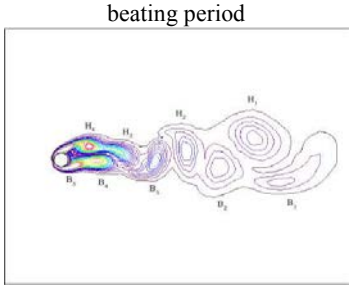

$t_o + 7/3T_o$

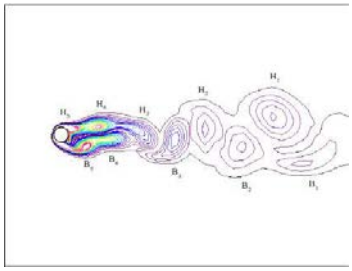

$t_o + 8/3T_o$

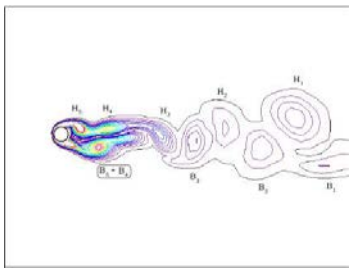

$t_o + 3T_o$

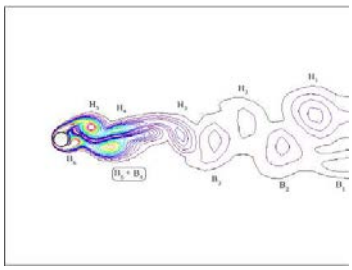

$t_o + 10/3T_o$

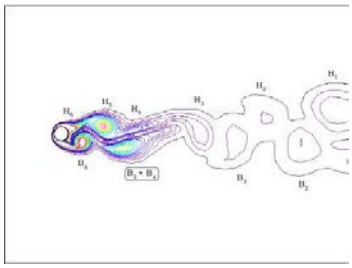

$t_o + 11/3T_o$

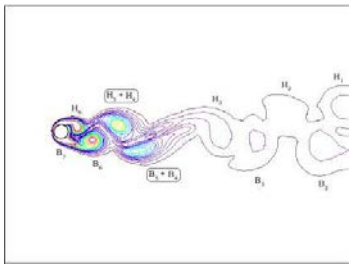

$t_o + 4T_o$

Figure 11. Details of the vortex merging mechanism associated with the beating behaviour at F=1.25

Figure 11 shows the fluctuations of the lift (blue) and drag (red) coefficients over a whole beating period. The circles represent the time steps used for the visualizations in the rest of the Fig. 11. At $t_o + 2T_o$, the vortices are shed alternately from the upper and lower side of the cylinder, as in the classical 2S mode. On the following snapshot, it is clear that the vortices B_3 and B_4 are distinct, as they have been shed over two successive cycles. The situation is identical in the upper

side with the vortices H_3 and H_4. At $t_o + 3T_o$, the vortices B_4 and B_5 begin to merge: B_4 is not energetic enough and cannot be inserted between H_3 and H_4. Vortex B_4 is therefore swallowed by B_5, and the pure sinusoidal response of the 2S mode is lost. The fusion goes on until the two vortices form only one structure called B_5+B_4. The phenomenon destabilizes the upper side of the wake: as B_4 is not between H_3 and H_4, it prevents H_4 to be convected downstream as long as the structure B_5+B_4 is not completely merged. A similar coalescence phenomenon appears thereby in the upper side and gives birth to the structure H_5+H_4. This merging could be related to the C(2S) mode of Williamson and Roshko [24] in which a coalescence of the classical 2S streets appears.

An important consequence of the merging is the modification of the longitudinal space between the vortices. At $t_o + 2T_o$, the vortices are regularly spaced out, whereas at $t_o + 4T_o$ a group of structures is concentrated in the near wake. This accumulation of vortices in the near wake explains why the lift and drag coefficients are greater at these moments. Indeed, the forces exerted on the cylinder are more important when the vortices are merging, because the fusion delays the shedding and leads to the accumulation of vortices in the near wake.

Case $F = 1.25$ is situated on the upper limit of the lock-in zone and the beating behaviour could also be interpreted as a transition between a locked and unlocked wake. However, this phenomenon is still present at $F = 1.50$ or $F = 0.50$, i.e. really outside the lock-in zone. The lock-in zone could thus be characterized as the domain where the wake reponse is purely sinusoidal and governed by the forced oscillation frequency. Outside of it, the wake seems to loose its sinusoidal form and vortex merging phenomena are observed. For relatively small amplitude of oscillation (like the one chosen here, $A = 0.25$), we did not observe a "true" modification of the vortex shedding mode: the emission remains close to the classical 2S mode, but this emission is sinusoidal or not depending on whether the wake is synchronized or not. Our results corroborates other studies, such as [1], in which a change in the vortex shedding mode has not been observed either, but exhibited a vortex merging phenomenon for oscillation amplitudes of the same order as in the present case ($A < 0.50$). In the following, the 2P and P+S modes are tried to be simulated, by choosing greater amplitudes of oscillation for which the vortex shedding modes are clearly distinct.

- **2P like vortex shedding mode**

The values used to investigate other shedding modes are deduced from the vortex shedding map proposed by Williamson & Roshko [24]. The couple $(A, F) = (1.00, 0.90)$ is chosen in the middle of the 2P shedding mode domain.

The wake looks like a 2S shedding mode but the vortices are stretched in the vertical direction because of the higher amplitude of oscillation. And yet if we look in details at the wake structure, it is possible to discern a secondary vortex, whose intensity is very small. At $t = t_o$ on Fig. 12, the vortex V_1 seems to have a tail which is composed of the small vortex V_2. Although V_2 is over V_3 at $t = t_o$, the small vortex V_2 slips progressively over V_3 and is then attached to V_1. The same process appears for V_3 and V_4: as the vortex V_5 has not been inserted between V_3 and V_4, the small vortex V_4 slips over V_5 and attaches to the tail of V_3.

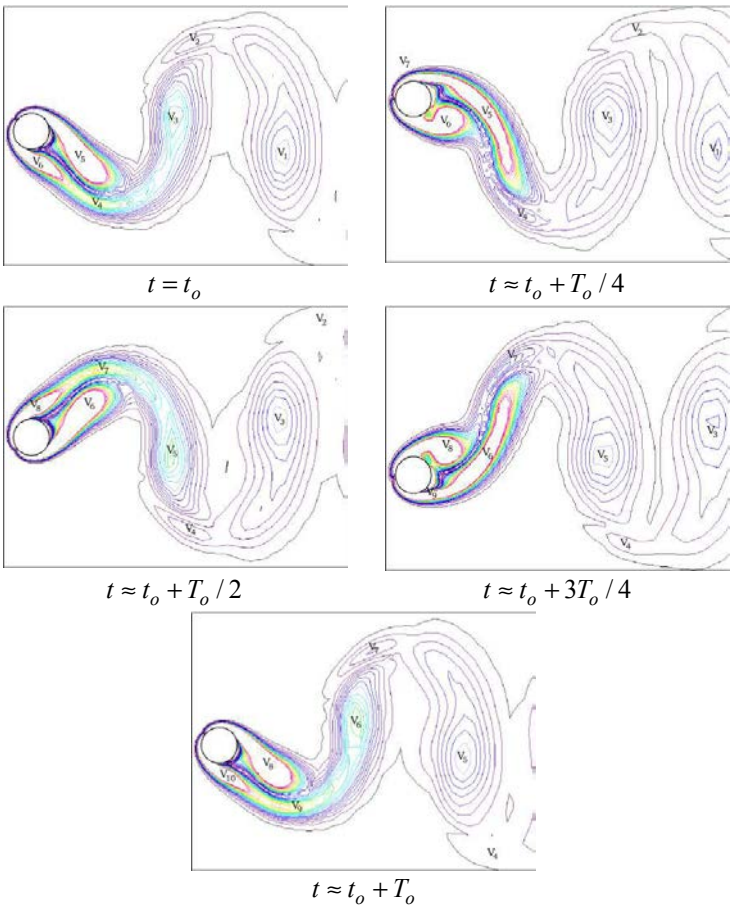

Figure 12. 2P like shedding mode for (*A;F*)=(1.00,0.90)

The vortices are still alternately shed from the upper and lower side of the cylinder as in a 2S mode, but as they move downstream, a weakly energetic vortex slips over its following neighbour and forms the tail of its preceding neighbour. The vortices are then assembled by asymmetric pairs. Over one cycle period, two pairs (here V_4+V_5 and V_6+V_7) are shed, so the vortex shedding mode looks like a 2P mode in which the vortices would not be identical in a same pair. As the small vortex is weakly energetic, it quickly disappears in the far wake. The vortex shedding mode obtained in the far wake looks therefore like a 2S mode with deformed vortices.

It is not surprising to obtain a deformed shedding mode instead of the regular 2P mode. The reason comes certainly from the fact that the Reynolds number used here is relatively small. As already mentioned, the vortex shedding modes are quite different at low Reynolds numbers. Indeed, it has been noted [12] that the 2P is not observed at low Reynolds numbers but the reasons why the wake is different remain obscure. Experiments presented in [17] exhibited only the P+S mode for $\mathrm{Re} < 190$; the 2P mode in their laminar-regime studies has nonetheless never been observed.

Finally, it should be mentioned that the vortex shedding process shown on Fig. 12 respects the lock-in behaviour: the cycle period is T_o, i.e. the forced oscillation period. The FFT of the lift coefficient would show only one peak at $f^* = 1$.

- **P+S vortex shedding mode**

The choice of the oscillation parameters is still based on the Williamson-Roshko map. Thus the couple $(A, F) = (1.25, 1.50)$ is located in the middle of the P+S shedding mode. The wake is now composed of two distinct rows of vortices. In the upper row, the vortices are grouped by pairs (P) whereas a single vortex (S) is shed in the lower row. The configuration of the wake is shown on Fig. 13. It should be noted that the cycle period of the wake is T_o, i.e. the forced oscillation period. The wake is however not locked because the spectrum of the lift coefficient does not contain only one peak. This was already the case for $F = 1.50$ and $A = 0.25$. A major difference between these two cases concerns the position of the second peak relative to the first. For a small amplitude of oscillation $A = 0.25$, the second peak is a low-frequency peak. As a result, a low-frequency beating behaviour is observed (Fig. 14, top): the fluctuations of the lift are not periodic over one period T_o but over several periods. On the contrary, for $A = 1.25$, the secondary peak in the spectrum is a high frequency peak. The fluctuations of the lift are therefore modulated by a signal which influences the response during one cycle T_o (Fig. 14, bottom). The fluctuations of the lift are periodic between two successive cycles, but over one cycle, a small fluctuation is observed. We suppose that this fluctuation could be related to the emission of the pair in the upper side of the wake.

The influence of the amplitude on the vortex shedding mode is crucial. Indeed, according to the values, high- or low-frequency phenomena are observed. For small amplitudes, the low-frequency leads to a vortex merging in the wake, which is associated with a beating behaviour in the time histories of C_L. On the contrary, for high amplitudes, the high frequency phenomenon leads to the emission of a pair of vortices in the upper side of the wake, which could be related to the modulation observed in the time evolution of the lift coefficient.

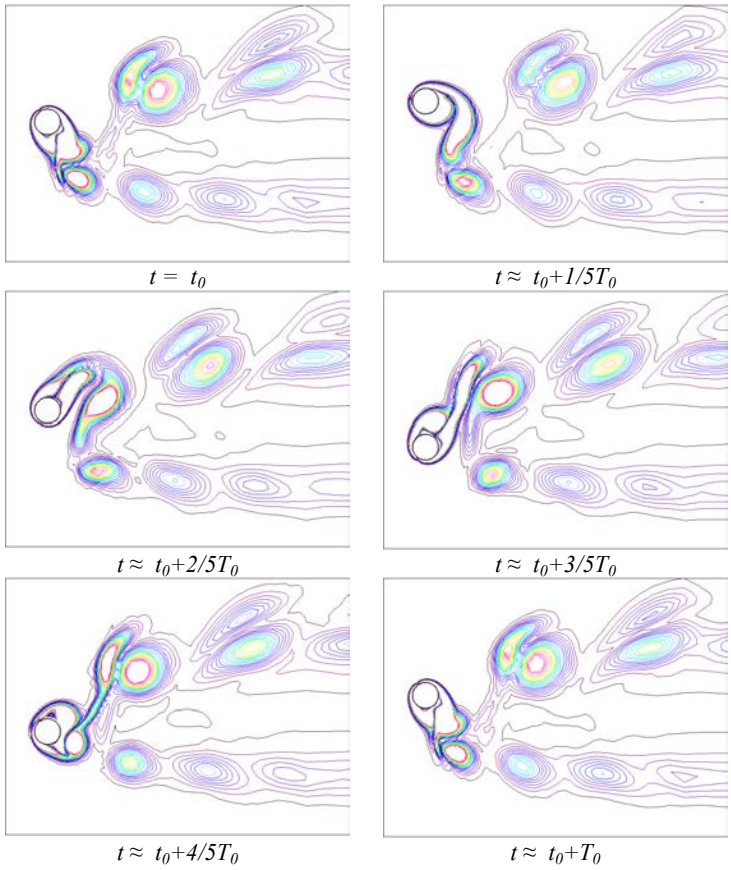

Figure 13. P+S vortex shedding mode for A=1.25 and F=1.50

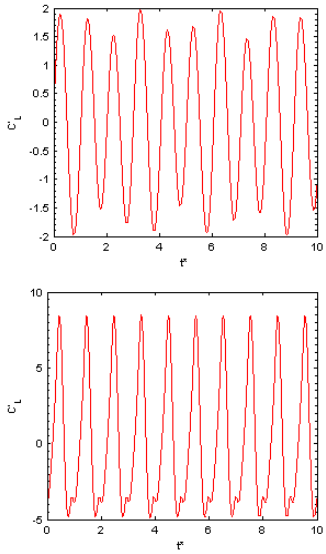

Figure 14. Time evolution of the lift coefficient for F=1.50. A=0.25 (top) , A=1.25 (bottom)

5. CONCLUSION

The present work has shown that the phenomena commonly observed in the case of a cylinder forced to oscillate in a transverse flow can be predicted with our industrial code, however small the CPU time may be (about 2.5 days). The first task of validation for the fixed cylinder demonstrates the ability of the code to provide a rather accurate description of the flow. The vortex shedding modes observed with forced oscillations have been related to the frequency content of the lift coefficient spectrum. The influence of the amplitude has been investigated and we have been able to observe the modification of the vortex shedding mode according to the value of A and F.

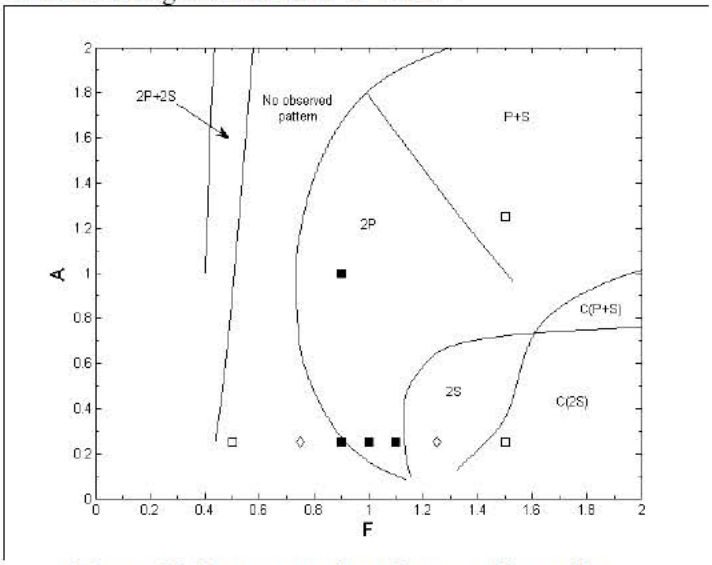

Figure 15. Representation of our results on the Williamson-Roshko vortex shedding mode map adapted in a F-scale

Although the 2P shedding mode has not been obtained (certainly because of our low Reynolds number), the other classical 2S, P+S and C(2S) modes have been found. The different simulations performed in this study are summarized on the Williamson-Roshko map adapted in an F-scale and sketched in Fig. 15. The filled squares indicate that lock-in is observed, whereas the empty ones mean that the wake is desynchronized. Simulations at the limits of the lock-in zone are identified with the lozenges.

REFERENCES

[1] P. ANAGNOSTOPOULOS. Numerical Study of the Flow Past a Cylinder Excited Transversely to the Incident Stream. Part 1: Lock-In Zone, Hydrodynamic Forces and Wake Geometry. *Journal of Fluids and Structures*, **14**, 819-851, 2000.

[2] M. BRAZA, P. CHASSAING, H. HA MINH. Numerical Study and Physical Analysis of the Pressure and Velocity Fields in the Near Wake of a Circular Cylinder. *Journal of Fluids Mechanics*, **165**, 79-130, 1986.

[3] J. CARBERRY, J. SHERRIDAN, D. ROCKWELL. Force and Wake of an Oscillating Cylinder. *Journal of Fluids and Structures*, **15**, 523-532, 2001.

[4] S.C.R. DENIS, G-Z. CHANG. Numerical Solutions for Steady Flow Past a Circular Cylinder at Low Reynolds Numbers up to 100. *Journal of Fluids Mechanics*, **42**, 471-489, 1970.

[5] S. DONG, G.E. KARNIADAKIS. DNS of Flow Past a Stationary and Oscillating Cylinder at Re=10 000. *Journal of Fluids and Structures*, **20**, 519-531, 2005.

[6] C. FARHAT, M. LESOINNE, P. STERN. High Performance Solution of Three-Dimensional Non-Linear Elastic Problems via Parallel Partitioned Algorithms: Methodology and Preliminary Results; *Advances in Engineering Software*, **28**, 43-61, 1997.

[7] J.H. FERZIGER, M. PERIC. *Computational Methods for Fluid Dynamics*. Springer-Verlag, 1996.

[8] U. FEY, M. KÖNIG, H. ECKELMANN. A New Strouhal-Reynolds-Number Relationship for the Circular Cylinder in the Range $47<Re<2.10^5$. *Journal of Physics Fluids*, **10** (7), 1547-1549, 1998.

[9] M.S. GEROUACHE. *Etude numérique de l'instabilité de Bénard-Karman derrière un cylindre fixe ou en mouvement périodique. Dynamique de l'écoulement et advection chaotique*. PhD Thesis, Ecole Polytechnique de l'Université de Nantes, 2000.

[10] R.D. HENDERSON. Details of the Drag Curve Near the Onset of Vortex Shedding. *Physics of Fluids*, **7** (9), 2102-2104, 1995.

[11] D. JEON, M. GHARIB. On Circular Cylinders Undergoing Two-Degree-of-Freedom Forced Motions. *Journal of Fluids and Structures*, **15**, 533-541, 2001.

[12] A. KHALAK., C.H.K. WILLIAMSON. Motions, Forces and Mode Transitions in Vortex-Induced Vibrations at Low Mass-Damping; *Journal of Fluids and Structures*, **13**, 813-851, 1999.

[13] G.H. KOOPMANN. The Vortex Wakes of Vibrating Cylinders at Low Reynolds Numbers; *Journal of Fluid Mechanics*, **27**, 501-512, 1967.

[14] M.R.H. NOBARI, H. NAREDAN. A Numerical Study of Flow Past a Cylinder with Cross Flow and Inline Oscillation. *Computers and Fluids*, **35**, 393-415, 2006.

[15] C. NORBERG. Fluctuating Lift on a Circular Cylinder: Review and New Measurements. *Journal of Fluids and Structures*, **17**, 57-96, 2003.

[16] S. PIPERNO. *Simulation numérique de phénomènes d'interaction fluide-structure*. PhD Thesis, Ecole Nationale des Ponts et Chaussées, 1995.

[17] S.E. RAMBERG, O.M. GRIFFIN. Hydroelastic Response of Marine Cables and Risers. *Hydrodynamics in Ocean Engineering*, 1223-1245, 1981.

[18] A. ROSHKO. *On the Development of Turbulent Wakes From Vortex Streets*. Naca Report, 1191, 1954.

[19] J.F. SIGRIST. *Modélisation et simulation numérique d'un problème couplé fluide/structure non-linéaire. Application au dimensionnement de structures nucléaires de propulsion navale*. PhD Thesis, Université de Nantes, 2004

[20] J.F. SIGRIST, D. ABOURI. *Numerical Simulation of a Non-Linear Coupled Fluid-Structure Problem with Implicit and Explicit Coupling Procedures*. Pressure Vessel and Piping, Vancouver, 22-28 July 2006.

[21] M. SAGHAFIAN, P.K. STANSBY, M.S. SAIDI, D.D APSLEY. Simulation of Turbulent Flows Around a Circular Cylinder Using Nonlinear Eddy–Viscosity Modelling: Steady and Oscillatory Ambient Flows. *Journal of Fluids and Structures*, **17**, 1213-1236, 2003.

[22] C.H.K. WILLIAMSON. Defining a Universal and Continuous Strouhal-Reynolds Number Relationship for the Laminar Vortex Shedding of a Circular Cylinder at Low Reynolds Numbers. *Journal of Physics Fluids*, **31**, 27422, 1988.

[23] C.H.K. WILLIAMSON. Advances in Our Understanding of Vortex Dynamics in Bluff Body Wakes. *Journal of Wind Engineering and Industrial Aerodynamics*, **69-71**, 3-32, 1997.

[24] C.H.K. WILLIAMSON, A. ROSHKO. Vortex Formation in the Wake of an Oscillating Cylinder. *Journal of Fluids and Structures*, **2**, 355-381, 1988.